Nanosizing palladium on P_xO_y incorporated holey graphene sheets for effective formic acid oxidation

*Juan Wang[†a], Detre Teschner[b], Xing Huang[*b], Yuanying yao[†a], Marc Willinger[b], Lidong Shao[*a], and Robert Schlögl[b]*

[a]Shanghai Key Laboratory of Materials Protection and Advanced Materials in Electric Power, Shanghai University of Electric Power, 2103 Pingliang Road, Shanghai 200090, China. [b]Department of Inorganic Chemistry Fritz-Haber Institute of the Max Planck Society Faradayweg 4-6, 14195 Berlin, Germany.

*Corresponding author: lidong.shao@shiep.edu.cn (L.D.S.)

xinghuang@fhi-berlin.mpg.de (X.H.)

[†]Juan Wang and Yuanying Yao contributed equally to this work.

ABSTRACT: A stack of basic structural carbon units with phosphorus oxides (P_xO_y) incorporated at edges and internal defects is obtained and applied as a support material for Pd nanoparticles to create an efficient electrocatalyst for HCOOH oxidation. In contrast to the lack of activities displayed by Pd supported on lyophilized and vacuum annealed graphene oxides, Pd on P_xO_y incorporated holey graphene sheets (Pd/HGP_xO_y) shows efficient activity and stability in HCOOH oxidation. Surface analysis of fresh and reacted catalysts reveal that HCOOH oxidation is favored by Pd/HGP_xO_y due to the decreased Pd electron density caused by the electron transfer from Pd to the HGP_xO_y.

KEYWORDS: holey graphene；P_xO_y incorporation；palladium nanoparticle；metal-support interaction；HCOOH oxidation

1. Introduction

Because of formic acid's lower crossover flux through Nafion membranes compared to that of methanol, formic acid fuel cells offer exciting prospects for powering portable electronic devices [1]. Additionally, Pd-anode catalysts show greater electrocatalytic activities for direct formic acid fuel cells with lower costs than Pt-based catalysts [2]. However, because of the ease of Pd oxidation, the electrocatalytic stability of Pd catalysts is not satisfactory. Secondary metals are commonly used to modify the electronic properties of Pd by forming alloys such as Pd-Co [3], Pd-Ni [4], and Pd-Au [5]. However, the erosion of binary-metal-alloy catalysts in the acidic environment of fuel cells weakens the activities of these catalysts.

Recent works have reported that P doping can effectively improve the electrocatalytic activities of Pt and Pd catalysts. For example, C-supported Pt-Ru-P [6], Pt-Sn-P [7], Pt-P [8], Pd-PCNTs [9] and Pd-P [10] catalysts have been synthesised and used as anode or cathode electrocatalysts in fuel cells. For C-supported Pd-P catalysts [10], electrochemical measurements have shown that P doping can effectively promote formic acid electrooxidation through a direct pathway. However, modifying Pd with P on a C support for practical applications is challenging. First, the mechanism by which the P or P_xO_y modifications affect HCOOH oxidation remains unclear. In the electrochemical field, literatures report the existence of P as a simple substance and its interaction with C in forms of C-P bonds. Further interactions with supported

metal particles take place as P-Metal bonds. Such deductions, in a great number of works, are highly suspectable as we observed a high amount of P_xO_y in carbon networks even after high temperature reduction treatments. Second, the utilization of C supports inevitably increases the thickness of the diffusion layer, thereby enhancing the mass-transfer resistance of the fuel molecules [11].

2. Experimental Section

Preparation of Pd/HGP_xO_y and Pd/HG is described in the main content. Pd loading was prepared by the following route: palladium nitrate (ca. 40%Pd, Aldrich) was dissolved in ethanol and mixed with the supporting materials. Ultrasonication was carried out for 20 minutes and samples were dried by lyophilization. The samples were then collected and placed in furnace for reduction treatment at 200°C. X-ray diffraction (XRD) was performed using a Bruker D8 Advance XRD instrument with Cu-Kα radiation. An aberration-corrected JEOL JEM-ARM200CF transmission electron microscope was employed to investigate structural and chemical properties in STEM mode. X-ray photoelectron spectroscopy (XPS) was conducted with a Thermo ESCALAB 250 XPS instrument using a monochromatic Al Kα source (1486.6 eV).

3. Results and Discussion

In this work, graphite oxide was synthesized from purified natural graphite (SP-1, Bay Carbon) by the Hummers method [12]. Colloidal dispersion of graphene oxide (GO) sheets in water at the concentration of 0.5 g/L were prepared with the aid of two hours sonication. Digital photo of GO solution in Figure 1 was taken after one month keeping still. As shown in Figure 1, GO

was extracted from the aqueous solution by lyophilization and the obtained brown-color material is shown by image together with its SEM characterization. Subsequently, heating treatment was applied under vacuum at 300ºC, a digital photo of black-color material and its SEM image are shown in Figure 1. Further heating treatment was conducted at 1000ºC under H_2/He atmosphere with and without sodium hypophosphite (NaH_2PO_2) to obtain P_xO_y incorporated and unmodified graphene-based holey nanosheets (HGP_xO_y and HG). After the heating treatment in the presence of NaH_2PO_2, the obtained material was washed by distilled water for three times and dried under vacuum at 60ºC. SEM images of the two treated materials at 1000ºC (HG and HG P_xO_y) are shown in Figure 1.

Figure 2a shows the X-ray diffraction (XRD) patterns of fabricated materials in Figure 1. The peak at the lower $2\theta = 9.4°$ of lyophilized GO corresponded to an interlayer distance of 0.93 nm and resulted from the accommodation of various O-containing groups and water molecules during the graphite oxidation process [13,14]. After vacuum annealing treatments, the absence of the 004 (21.6°), 100 (43.3°), and 101(44.5°) peaks shows that the materials are largely X-ray amorphous turbostratic mixture of basic structural units with many internal lattice defects. Meanwhile, the absence of Pd peaks is due to the low loading of Pd dispersed in nanoscale size ranges.

The structural evolution occurring during the lyophilization and heating processing are also reflected in their Raman spectra (Figure 2b). After the

1000ºC annealing treatment, the ID/IG intensity ratio of HG and HGP_xO_y increased compared to that in GO obtained in step a and b. This change suggests holey structural units with increased internal lattice defects upon reduction of the GO.

Pd with a large dispersion and narrow size distribution (3.3±0.2 nm) was then deposited onto the HG and HGP_xO_y supports in low loadings (3±0.2wt% measured by inductively coupled plasma (ICP)). To investigate the support effect, lyophilized GO (step a) and vacuum treated GO (step b) were used to support Pd. Figure 2c displays a high-resolution transmission electron microscopy (HRTEM) image of a metallic Pd particle with distinct edges on HGP_xO_y. The crystal planes and interplanar distances, as well as the acute angles, are labeled adjacent to the corresponding Pd particle. The insets show the fast Fourier transform of the local HRTEM image and the size distribution of the Pd particles.

For the purpose of identifying the chemical state of P compounds, X-ray photoelectron spectroscopy (XPS) was used to analyze the Pd/HGP_xO_y. The P 2p XPS spectrum shows peaks at 133.6 eV and 132.7 eV in Figure 2d. The P2p peak around 133.6-134.7eV can be assigned to $(PhO)_3PO$ (Ph represents the phenyl group,-C_6H_5) when the P atom is bonded to four O atoms by one double bond and three single bonds [15]. When P is bonded to one C atom and three O atoms (e.g., in $CH_3OP(OH)_2$), the P2p peak moves to ca.133.6eV [16]. The above assignment suggests that, in our work, P deposit is mainly present on the

carbon in its oxidized form (P_xO_y). Scanning transmission electron microscopy (STEM)-energy-dispersive X-ray (EDX) analyses and elemental maps of individual Pd nanoparticles (PdNPs) showing the C, O, P, and Pd distributions on the HGP_xO_y indicate that the incorporated elements are homogeneously distributed (Figure 2e-h).

Typical cyclic voltammograms (CVs) behaviors of formic acid electrooxidation (FAO) in a 0.5-M HCOOH + 0.5-M H_2SO_4 electrolyte solution are shown in Figure 3a. The anodic peak current density on the Pd/HGP_xO_y catalyst was 728.34 A/g, which was 2.16 times as that of Pd/HG. Moreover, the oxidation peak of Pd/HGP_xO_y is approximately 69 mV vs. SCE, while that of Pd/HG is about 139 mV vs. SCE. The highly negative peak potential (70 mV vs. SCE) indicated the excellent catalytic property of the Pd/HGP_xO_y catalyst. The accurate electrochemical surface area (ECSA) obtained from CO-stripping experiments (Figure 3c and 3d) were used to calculate the specific activity for catalyst. The specific activities for catalysts were shown in Figure 3e and 3f. Pd/HGP_xO_y exhibited a better electrocatalytic specific activity (15.43 A/m^2) than Pd/HG (11.23 A/m^2). The peak potential of the absorbed CO is commonly used as a tool to compare the anti-poisoning ability [17]. The peak potential of Pd/HGP_xO_y is negative than that of Pd/HG indicating after P_xO_y incorporation into the holey graphene sheets (Figure 3c and 3d), indicates that the anti-poisoning ability has been greatly enhanced. The Pd/HGP_xO_y has better catalytic stability than that of Pd/HG, based on chronoamperometric (CA) measurements at constant potential 70 mV (Figure 3 f) for 3600s.

Herein, reacted catalysts were collected after running multi-CV tests for 25 cycles and studied by the X-ray photoelectron spectroscopy (XPS). The Pd 3d core-level XPS spectra of the reacted Pd/HGP$_x$O$_y$ are shown in Figure 4c. The distribution of Pd species remained similar, indicating that Pd is reasonably stable. However, in the case of Pd/HG, reaction clearly affected the Pd 3d profiles, suggesting the occurrence of dynamic changes on the Pd surfaces of Pd/HG during the catalysis of HCOOH oxidation. Moreover, the shift of the Pd 3d spectrum in the reacted Pd/HGP$_x$O$_y$ (337.4 eV) in comparison to the reacted Pd/HG (337.1 eV) clearly indicates an interfacing interactions caused by the electron transfer from Pd to the HGP$_x$O$_y$.

P$_x$O$_y$ incorporation creates anchoring points for interactions with the Pd precursors. Hydrolysis treatments are applied to crystallize the embedded precursors to form nanocrystals [18]. XPS studies indicate a decrease in the 4d-electron density of Pd caused by electron donation from the metal to the P$_x$O$_y$ incorporated holey graphene sheets. Pd, with its decreased 4d-electron density, binds the COOH intermediate relatively weakly, and thus, the surface (COOH)ads coverage is reduced. Therefore, HCOOH is more easily oxidized through the direct pathway. Moreover, because heteroatoms are usually covalently bonded within the C frameworks, the interfacial interactions and the effects they induce should be sufficiently stable to persist throughout long-term reaction operations, as demonstrated by the preserved Pd 3d profile of the Pd/HGP$_x$O$_y$ catalyst.

CONCLUSIONS

In summary, P_xO_y incorporated holey graphene sheets were synthesized and applied as a support material for PdNPs to create anode catalysts for HCOOH oxidation. Improved activity and stability were achieved in comparison to those of the unmodified counterpart (Pd/HG). Surface analyses of fresh and reacted catalysts revealed that the decrease in the electron density of Pd favored the direct pathway of HCOOH oxidation. Applying HGP_xO_y as a support material for Pd has three obvious advantages for HCOOH oxidation applications. First, the use of a network of graphene-based nanosheets decreases the thickness of the diffusion layer and thereby reduces the mass-transfer resistance of fuel molecules and products. Second, reduction treatments during the annealing process restore the π- conjugated structures and enable obtained HG and HGP_xO_y to support low loadings of Pd for catalyzing reactions. Third, P_xO_y incorporation provides an economical alternative for modifying the electronic properties of the Pd surface in comparison to adding secondary metals**.**

Acknowledgments: This work was financially supported by the Shanghai Key Laboratory of Materials Protection and Advanced Materials in Electric Power, National Natural Science Foundation of China (21403137).

References

[1] J. Chang, L. Feng, C. Liu, W. Xing, X. Hu, An effective Pd-Ni_2P/C anode catalyst for direct formic acid fuel cells, Angew. Chem., Int. Ed., 53 (2014) 122-126.

(2) Z. Liu, H. Liang, Tham, M. P., Lim, T. H., Jiang, H. Nanostructured Pt/C and Pd/C catalysts for direct formic acid fuel cells. J. Power Sources 2006, 161, 831-835.

(3) Wang, R., Liao, S., Shan, J. High performance pd-based catalysts for oxidation of formic acid. *J. Power Sources* **2006**, *180*, 205-208.

(4) Li, R., Wei, Z., Huang, T., Yu, A. Ultrasonic-assisted synthesis of Pd-Ni alloy catalysts supported on multi-walled carbon nanotubes for formic acid electrooxidation. *Electrochim. Acta* **2011**, *56*, 6860-6865.

(5) Chiou, Y., Chen, K., Lin, H., Liou, W., Liou, H., Wu, S., Mikolajczuk A., Mazurkiewicz, M., Malolepszy, A., Stobinski, L., Borodzinski, A., Kedzierzawski, P., Kurzydlowski, K., Chien, S., Chen, W. Electrocatalytic properties of hybrid palladium-gold/multi-walled carbon nanotube materials in fuel cell applications. *Phys. Status Solidi A* **2011**, *208*, 1778-1782.

(6) Xue, X., Ge, J., Liu, C., Xing, W., Lu, T. Novel chemical synthesis of Pt-Ru-P electrocatalysts by hypophosphite deposition for enhanced methanol oxidation and co tolerance in direct methanol fuel cell. *Electrochem. Commun.* **2006**, *8*, 1280-1286.

(7) Xue, X., Ge, J., Tian, T., Liu, C., Xing, W., Lu, T. Enhancement of the electrooxidation of ethanol on Pt-Sn-P/C catalysts prepared by chemical deposition process. *J. Power Sources* **2007**, *172*, 560-569.

(8) Suzuki, S., Ohbu, Y., Mizukami, T., Takamori, Y., Morishima, M., Daimon, H., Hiratania, M. Platinum-phosphorus nanoparticles on carbon supports for oxygen-reduction catalysts. *J. Electrochem. Soc.* **2008**, *156*, B27-B31.

(9) Xin, Z., Wang, S., Wang, J., Huang, X., Ji, X., Yao, Y., Shao, L. Nanosizing low-loading Pd on phosphorus-doped carbon nanotubes for enhanced HCOOH oxidation performance. *Electrochem. Commun.* **2016**, *67*, 26-30.

(10) Yang, G., Chen, Y., Zhou, Y., Tang, Y., Lu, T. Preparation of carbon supported Pd-P catalyst with high content of element phosphorus and its electrocatalytic performance for formic acid oxidation. *Electrochem. Commun.* **2010**, *12*, 492-495.

(11) Chan, L., Allen, R. G., Scott, K. Effect of dispersion methods of an unsupported Pt-Ru black anode catalyst on the power performance of a direct methanol fuel cell. *J. Power Sources* **2006**, *161*, 11-18.

(12) Hummers, W. S., Offeman, R. E. Preparation of graphitic oxide. *J. Am. Chem. Soc*. **1958**, *80*, 1339.

(13) Yeh, T. F., Syu, J. M., Cheng, C., Chang, T. H., Teng, H. Graphite oxide as a photocatalyst for hydrogen production from water. *Adv. Funct. Mater*. **2010**, *20*, 2255-2262.

(14) Hailiang, W., Joshua Tucker, R., Xiaolin, L., Hongjie, D. Solvothermal reduction of chemically exfoliated graphene sheets. *J. Am. Chem. Soc.* **2009**, *131*, 9910-9911.

(15) Moulder, J. F.; Stickle, W. F.; Sobol, P. E.; Bomben, K. D. Handbook of X-ray photoelectron spectroscopy. Perkin-Elmer Corporation: Eden Prairie, MN, 1992.

(16) Wu, X., Radovic, L. R. Inhibition of catalytic oxidation of carbon/carbon composites by phosphorus. *Carbon* **2006**, *44*, 141-151.

(17) Zhou, W. P., Lewera, A., Larsen, R., Masel, R. I., Bagus, P. S., Wieckowski, A. Size effects in electronic and catalytic properties of unsupported palladium nanoparticles in electrooxidation of formic acid. *J. Phys. Chem. B* **2006**, *110*, 13393-13398.

(18) Friedrich, M., Kunkes, E., Rosenthal, D., Girgsdies, F., Zhang, B. S. Strong metal–support interactions between palladium and iron oxide and their effect on CO oxidation. *J. Catal.* **2014**, *317*, 220-228.

Figure captions

Figure 1. Digital photos and SEM images of obtained materials based on GO water solution.

Figure 2. a) XRD and b) Raman profiles with a, b, c, d corresponding to the obtained materials of step (a), step (b), step (c), and step (d) in Figure 1. e is Pd supported on HG, and f is Pd supported on HGP_xO_y. c) HRTEM images of supported Pd particles. The insets show (top left) the fast Fourier transform of the local HRTEM image and (bottom) the Pd particle size distribution on HGP_xO_y. d) XPS profile of P2p region of Pd/HGP_xO_y. e, f, g, h) STEM EDX mapping of Pd/ HGP_xO_y.

Figure 3. a) Mass activities for formic acid oxidation on Pd/HGP_xO_y and Pd/HG at a scan rate of 50 mV/s. b) the magnification of figure 3 a). c) and d) CO stripping measurements for Pd/HGP_xO_y and Pd/HG catalysts. e) Specific activities for formic acid oxidation on Pd/HGP_xO_y and Pd/HG at a scan rate of 50 mV/s. f) Chronoamperometry curves of the catalysts at constant potential.

Figure 4. XPS analysis of Pd 3d region: a) fresh Pd/HGP_xO_y, b) fresh Pd/HG, and c) reacted Pd/HGP_xO_y, d) reacted Pd/HG.

Figure1

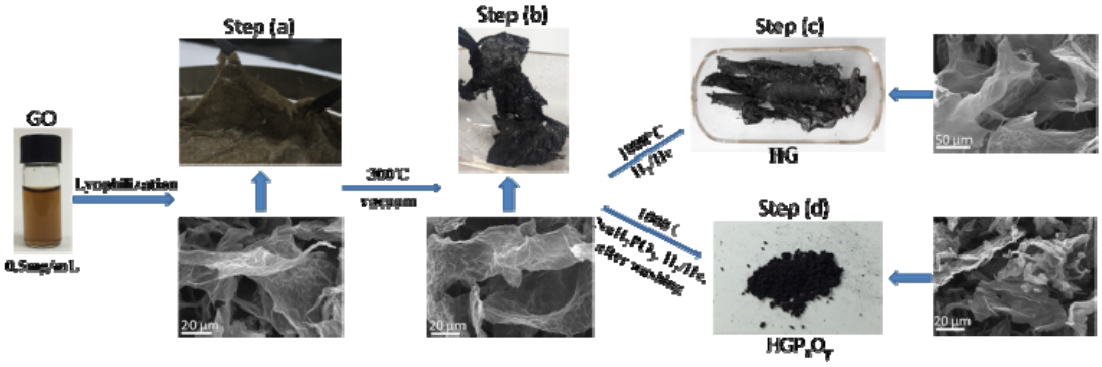

Figure 2

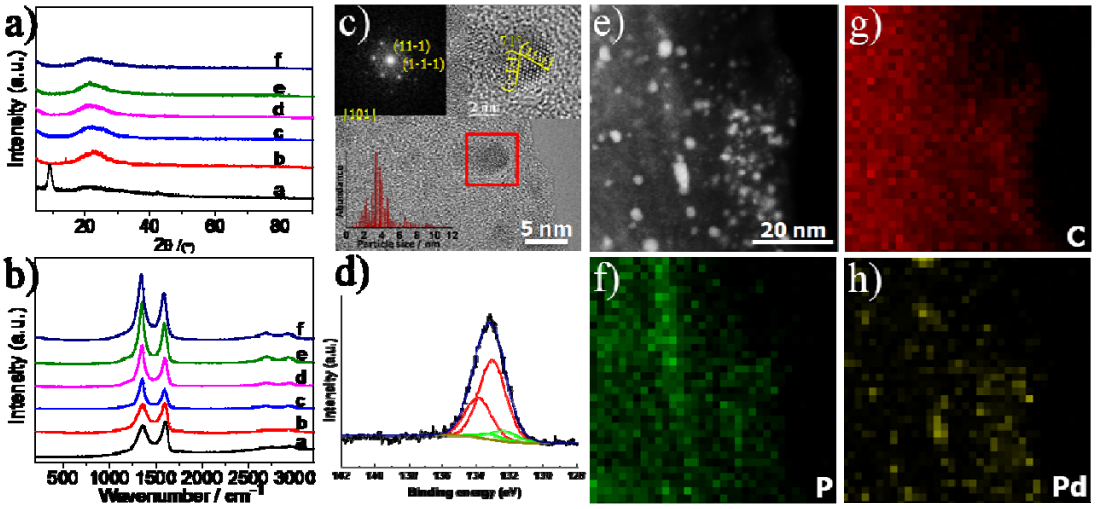

Figure 3

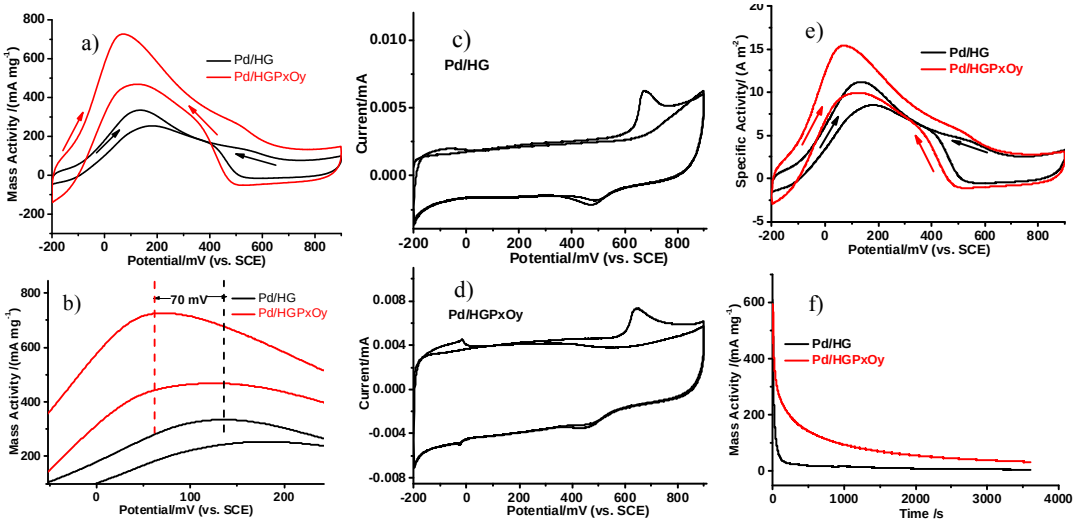

Figure 4